Chapter 7

Non-Destructive Surface Analysis by Low Energy Electron Loss Spectroscopy

Vitaliy Tinkov

Additional information is available at the end of the chapter

http://dx.doi.org/10.5772/48090

1. Introduction

The modern progress in such priority scientific directions as microelectronics, nanotechnology, material science, heterogeneous catalysis, etc., are impossible without obtaining quantitative information about physical–chemical properties from the nano-size near surface region of the materials.

It is known that the physical–chemical properties of the metallic alloy surfaces differ markedly from that of the bulk and, mainly, it is caused by segregation one of the alloy components on the surface [1]. It is related to the fact that the physical–chemical state of the surface substantially influences such surface processes as adsorption, catalysis, oxidation, friction and wear. Recently such phenomena as the thermo-induced surface segregation of alloy components as used for obtaining chemically-active surfaces have been widely used; being of great interest in terms of heterogeneous catalysis and the development of new nanotechnological processes. Study of the kinetics of surface segregation permits the determination of the bulk diffusion coefficients of the segregated elements; knowledge of which then permits the controlled change of surface structures under heat treatment and etc.

At the present for the investigation of the physical–chemical properties of the metallic alloy surfaces the nondestructive methods are widely used, such as an Rutherford Backscattering Spectrometry (RBS), X-ray Photoelectron Spectroscopy (XPS), Low Energy Ion Scattering (LEIS), Ultraviolet Photoelectron Spectroscopy (UPS) and other [2].

Physical phenomena such as secondary electron emission (SEE) can be used for investigation of the near surface region of a solid with a purpose to obtain quantitative information concerning its crystal structure, element composition and the electronic states of atoms [3,4]. On the Figure1 the total energy distribution of reflected SEE from a surface is shown which is irradiated by an electron beam of primary energy E_0. The shape is due to

some types of interaction: elastic and inelastic scattering together with secondary electron emission. There are four ranges in N(E), in each if which one of these interactions predominates.

The elastic interaction produced a narrow peak on the right, where the electrons retain their energy E_0 and merely show altered momentum direction (Region I). The broadening is due to thermal spread in the beam energy and is also affected by the analyzer resolution. With standard equipment the broadening is usually 0.5-1 eV, so phonon excitations (energy loss 10-50 meV) can be detected only by special techniques involving highly monoenergetic primary beams and improved analyzer resolution, as realized in high resolution energy loss spectroscopy. With other methods, one can assume that the elastic peak is due to group electrons from the beam that have undergone elastic and quasi elastic interactions with the surface. Various methods are applied to the elastic backscattering, particularly diffraction ones such as Low Electron Energy Diffraction (LEED) and high energy diffraction with back scattering which have been applied to the spatial distributions of the backscattered beams. The methods have been applied to the atomic structures and dynamic characteristics in ordered surface layers.

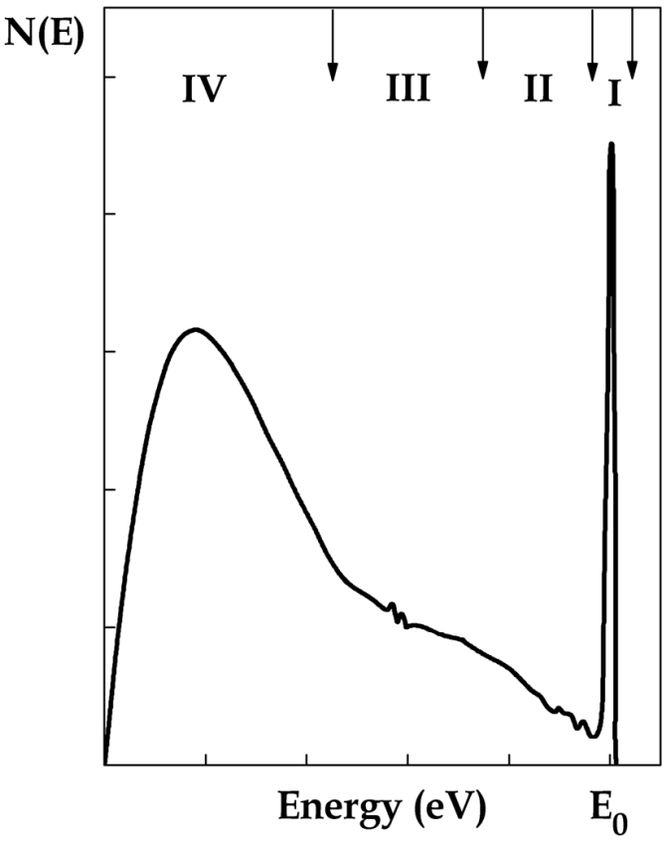

Figure 1. Total energy distribution of secondary electron emission from a surface which is irradiated by an electron beam of primary energy E_0

The broad low energy maximum (Region IV) is due to the true secondary electrons which have energies from zero up to some tens of eV and are formed by repeated inelastic

electron-electron scattering in the cascade process. The true secondary electrons may constitute up to 70% of total energy distribution. Their energy distribution is related to the random filling of the final states and to the cascade multiplication.

In Region III there is also a fine structure due to electrons from the solid escaping in the vacuum by the Auger process (Auger Electron Spectroscopy (AES)). The Auger electron spectrum for a given element has a characteristic form and certain energies which have meant that AES is widely used in elemental analysis.

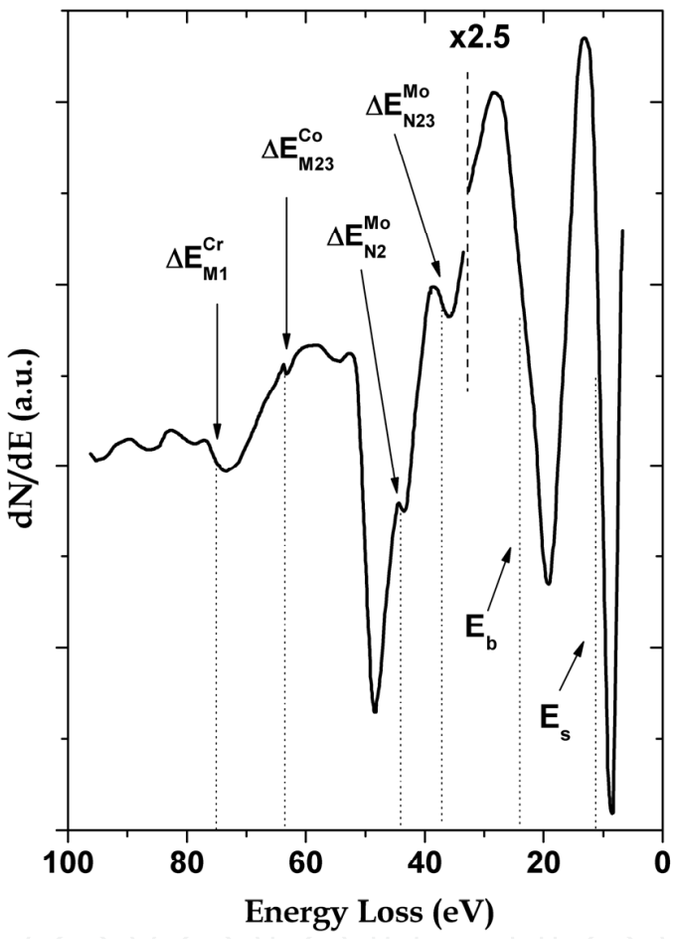

Figure 2. Example low EELS spectra obtained for the Co–Cr–Mo alloy surface at the primary energy E_0 = 350 eV with identification of energy losses

Region II is due manly to electrons that have lost some of their energy by inelastic scattering; directly by the elastic peak, one finds electrons that have suffered discrete energy losses from the excitation of inter- and intraband electronic transitions, surface and bulk plasmons, hybrid modes of plasmons and ionization losses (Ionization Spectroscopy). That range is usually 30-100 eV. Usually, the losses related to surface and bulk plasmon excitations are most intensive lines in the electron energy loss spectrum. The spectra of plasma oscillations are potential data carriers about composition and chemical state of elements on the surface of solid and in the adsorbed layers. The energy losses are called as characteristic losses because losses do not depend on the primary electron energy E_0 and its value is individual for the

chemical element and compound. Region II is called as Electron Energy Loss Spectroscopy (EELS). At energy $E_0 < 1000$ eV it can be called as low EELS. On the Figure 2 really low EELS spectra is shown with interpretation of losses for the Co-Cr-Mo alloy surface which was measured at the primary electron beam energy $E_0 = 350$ eV in dN/dE mode [5].

Ionization Spectroscopy (IS) is a variant on EELS. Gerlach et al. [6,7] first applied this in terms of analysis of the surface composition analysis for V, Ni, Pd and Mo as impurities on the surface of polycrystalline metals without depth analysis. The IS method is based on measuring the energy spectra of electrons, which have lost a particular portion of the energy ΔE for the excitation of electrons from internal atomic levels into the empty states (conduction band) of the solid. Having lost energy ΔE, and after being inelastically scattered, the primary electrons escape into vacuum and are registered on the background secondary emission spectrum as individual monochromatic groups which form spectral lines. The advantages of IS as compared to other methods of electronic spectroscopy are (i) the position of ionization lines in the spectrum with respect to the lines of elastic scattered electrons is determined by the binding energy of electrons in the ground state and by the distribution of the density of empty states and does not depend on the value of the primary electron energy E_0, (this allows easy separation of IS lines from the AES lines) and, (ii) the possibility to vary the probing depth of the near-surface region because the change in primary energy E_0 induces a change in the mean free path λ of electrons. On the Figure 3 the different between Auger process and ionization process is shown which are generated by an electron beam of primary energy E_0.

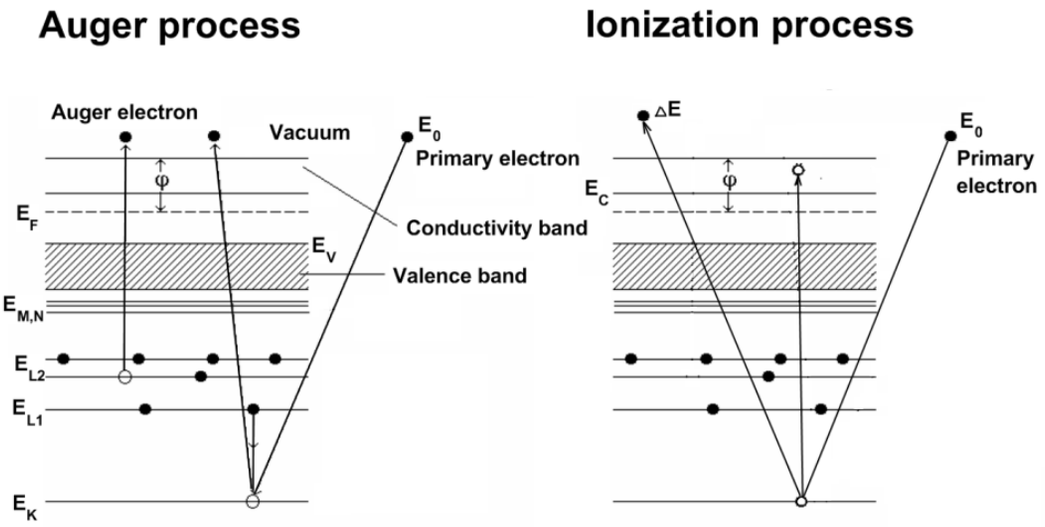

Figure 3. Example of different between Auger process and ionization process which are generated by an electron beam of primary energy E_0

The aim of the present chapter is to show the application of low Electron Energy Loss Spectroscopy as non-destructive method, namely Ionization Spectroscopy and surface and bulk plasmon excitations, at investigation of physical-chemical properties materials in the nano-size near surface region.

2. Low energy electron loss spectroscopy

2.1. Ionization spectroscopy

2.1.1. Physical model

Ionization Spectroscopy is based on the measurement of the energy spectra of electrons, which have lost a particular portion of the energy ΔE_β for the excitation of electronic transitions that are typical for a given kind of atom β. The position of an intensity line (IL) in the spectrum with respect to the primary electron energy E_0 is determined by the binding energy of electrons in the ground state and by the distribution of the density of empty states, but it does not depend on the value of E_0, on the work function or on the value of the surface charge.

The calculation of the contribution to the intensity of an IL by the electrons having lost an amount of energy ΔE_β at the depth Z from the sample surface by the ionization of the core states of the atoms β is simple when a traditional experimental configuration is used (an incident beam of the primary electrons is directed perpendicularly to the sample surface ($\theta_0 = 0$) and the secondary electrons are registered at the angle θ with respect to the normal). In this case calculations within the framework of a two-stage model allow us to obtain the following expression for the intensity of an IL [8]:

$$I_\beta\left(Z, E_{0j}\right) = K\sigma_\beta \tilde{r}_\beta n_\beta(Z)\exp(-Z/\Lambda_\beta)\,, \tag{1}$$

where K is an instrumental factor, σ_β is the ionization cross-section of the core level, $n_\beta(Z)$ is concentration of atoms β at depth Z from surface, $\tilde{r}_\beta$ is the elastic scattering factor of electrons. Λ_β is the effective free-path of electrons in a sample with respect to inelastic collisions, which is determined by the equation

$$\Lambda_\beta^{-1} = \lambda_0^{-1} + \left(\lambda_\beta \cos\theta\right)^{-1}. \tag{2}$$

For the Pt-Me (Me: Fe, Co, Ni, Cu) alloys [9]

$$\lambda_0 = \frac{1194}{E_{0j}^2} + 0.429E_{0j}^{1/2}\;;\; \lambda_\beta = \lambda(E_{0j} - \Delta E_\beta)\,.$$

An effective probing depth in IS amounts to ~ $3\Lambda_\beta$ because the secondary electrons created in the near-surface region of this thickness contribute for 95% to the total intensity of an IL. An increase of the effective probing depth upon increasing the energy E_0 also results in an increased contribution from the deeper layers of the concentration profile into the IL intensity. This enables us to carry out a layer-by-layer reconstruction of the concentration profiles of the elements using the energy dependencies of the IL.

After integration of Eq. (1) with respect to depth and spatial angle of the four-grid energy analyzer, an expression for the total IL intensity has the following form

$$I_\beta(E_0) = 2\pi K\sigma_\beta \int_0^\infty \int_{\Theta_{\min}}^{\Theta_{\max}} \tilde{r}_\beta n_\beta(Z)\exp(-Z/\Lambda_\beta)\sin\Theta dZ d\Theta\,, \tag{3}$$

where $\Theta_{min} = 4^o$ and $\Theta_{max} = 70^o$ are respectively the minimum and maximum values of polar angle for the standard quasi-spherical four-grid energy analyzer.

As pointed out above, the offered method is essentially not sensitive to the type of the energy analyzer used. Only the values of Θ_{min} and Θ_{max} that correspond to the concrete conditions of an experiment should be substituted in Eq. (3). In the case of a binary A-B alloy, usually the ratio of intensities of A to B

$$R_A(E_{0j}) = \frac{I_A(E_{0j}, \Delta E_A)}{I_B(E_{0j}, \Delta E_B)} \tag{4}$$

is measured experimentally in order to eliminate the instrumental factor K, which is often unknown.

Let us consider as new variables the relative concentrations of the elements in a layer with number i:

$$N_\beta(i) = n_\beta(i)\nu_\beta,\ \beta = \overline{A,B}\,, \tag{5}$$

where ν_β is the atomic volume of a pure component of an alloy. After replacing the integral in Eq. (3) by a summation over N and substituting the expression for I_β into formula (4), integration with respect to the width of isolated layer d leads to:

$$R_A(E_{0j}) = \frac{\sigma_A \lambda_i^A \nu_B}{\sigma_B \lambda_i^B \nu_A} \cdot \frac{\sum_{i=1}^{N} N_A(i) P_A(i, E_{0j})}{\sum_{i=1}^{N} N_B(i) P_B(i, E_{0j})}, \tag{6}$$

where

$$\begin{aligned} P_\beta(i, E_{0j}) &= \exp\left[-\frac{(i-1)d}{\lambda_0}\right] \int_{\Theta_{\min}}^{\Theta_{\max}} D_i(E_{0j}, \Theta)\tilde{r}_\beta \left[1 - \exp\left(-\frac{d}{\Lambda_\beta}\right)\right] d\Theta \\ D_i(E_{0j}, \Theta) &= \exp\left[-\frac{(i-1)d}{\lambda_0 \cos\Theta}\right] \frac{\cos\Theta \sin\Theta}{\lambda_0 + \lambda_i^\beta \cos\Theta}, \end{aligned} \tag{7}$$

i = 1, 2, ..., N - 1, and i = N

$$P_\beta(i, E_{0j}) = \exp\left[-\frac{(N-1)d}{\lambda_0}\right] \int_{\Theta_{\min}}^{\Theta_{\max}} D_N(E_{0j}, \Theta)\tilde{r}_\beta d\Theta, \tag{8}$$

Following the approach offered in [10], the expression (6) is transformed into a system of linear equations (SLE) with respect to $N_A(i)$ using the relation $N_A(i) + N_B(i) = 1$. As a result, we obtain (j = 1, 2, ..., M)

$$\frac{\sum_{i=1}^{N} N_A(i)\left\{\frac{\sigma_A \lambda_i^A \nu_B}{\sigma_B \lambda_i^B \nu_A} P_A(i, E_{0j}) + R_A(E_{0j}) P_B(i, E_{0j})\right\}}{\sum_{i=1}^{N} P_B(i, E_{0j})} = R_A(E_{0j}), \quad (9)$$

where E_{0j} is the energy of primary electrons for which we have measured the ratio of IL intensities $R_A(E_{0j})$. Assuming that all interlayer distances in the near-surface region of a single-crystal alloy are identical and equal to d, for summations in Eqs. (6) and (9) the number of terms is selected that corresponds to the selection of N monolayers parallel to a free surface, using the relationship $(N-1)\cdot d = 3\Lambda_{max}$ (where $\Lambda_{\max} = \left(\Lambda_A(E_0^{\max}) + \Lambda_B(E_0^{\max})\right)/2$). The system of linear equations (9) can be solved only when it is determined or overdetermined, i.e. if the inequality $M \geq N$ is true for this system.

In the following sections, methods are presented for building the solution of Eq. (9) and for the numerical calculation of the concentration profiles within the framework of the described model.

2.1.2. Layer-by-layer reconstruction methods

A system of equations, describing the deviations of the concentrations in a monolayer i ($N_A(i)$) from their bulk value N_A, can be represented in matrix form by the expression

$$\sum_{i=1}^{N} Q_{ji} \delta N_A(i) = \tilde{R}_A(E_{0j}), \quad (10)$$

where $\delta N_A(i) = N_A(i) - N_A$, $\tilde{R}_A(E_{0j}) = R_A(E_{0j}) - N_A \sum_{i=1}^{N} Q_{ji}$, and an explicit form of the matrix elements Q_{ji} is evident from the expression (9). However, the practical solution of the Eq. (10) presents particular difficulties because the matrix elements Q_{ji} correspond to close energy intervals that do not differ sufficiently. As a result, the determinant of the matrix Q is close to zero and the system (10) is ill-conditioned. As a consequence, the errors in the matrix elements Q_{ji} and in the $\tilde{R}_A$ values can result in an incorrect solution.

To construct a stable approximation for the solution of system (10), the condition-gradients projection method, the conjugate gradients projection method, the method of conjugate gradient projected on the Π^+–space and also the regularization method [11] were used in the present work. More detailed information on techniques for solving ill-posed problems can be found in [10,11]. The described regularization algorithm for the reconstruction of the elemental concentration profiles in a binary alloy on the basis of energy dependencies of the ratio of IL intensities is implemented in FORTRAN codes.

2.1.3. Results of the layer-by-layer reconstruction

Approbation of method of nondestructive layer-by-layer analysis was performed for the single crystal $Pt_{80}Co_{20}$ alloy with (100) and (111) surface orientations [12]. Initially, $Pt_{80}Co_{20}$(111) alloy surface was in a disordered state. First, we measured the spectra of the ionization losses for the clean (100) and (111) surfaces of $Pt_{80}Co_{20}$ alloy and polycrystals of platinum and cobalt in the dN/dE mode. The energy losses $\Delta E^{Pt}_{O_{2,3}} = 54eV$, $\Delta E^{Co}_{M_{2,3}} = 62eV$ and their IL were recorded in the range of primary electron energy E_0 = 200 - 500 eV.

In order to ignore in calculations an instrumental factor K (it is often unknown), the ionization cross-section σ_β and elastic scattering factor $\tilde{r}_\beta$ and the possible influence of matrix effects (for example, due to difference of atomic radii for platinum and cobalt r_{Pt}/r_{Co} = 1.104), usually the IL ratio of elements is measured, with normalization on standards by following equation:

$$R(E_0) = \frac{R_{alloy}(E_0)}{R_{st}(E_0)}, \tag{11}$$

where $R_{alloy}(E_0) = I^{alloy}_{Co}(E_0) \big/ I^{alloy}_{Pt}(E_0)$; $R_{st}(E_0) = I^{st}_{Co}(E_0) \big/ I^{st}_{Pt}(E_0)$; I^{alloy}_{Co}, I^{alloy}_{Pt} and I^{st}_{Co}, I^{st}_{Pt} are intensity lines of the ionization losses of the alloy components and standards (pure metals), respectively. Figure 4 shows the ratio of ionization peaks of Co to Pt as a function of the primary electron energy for (111) and (100) faces of $Pt_{80}Co_{20}$ alloy at room temperature before and after normalization on the standards.

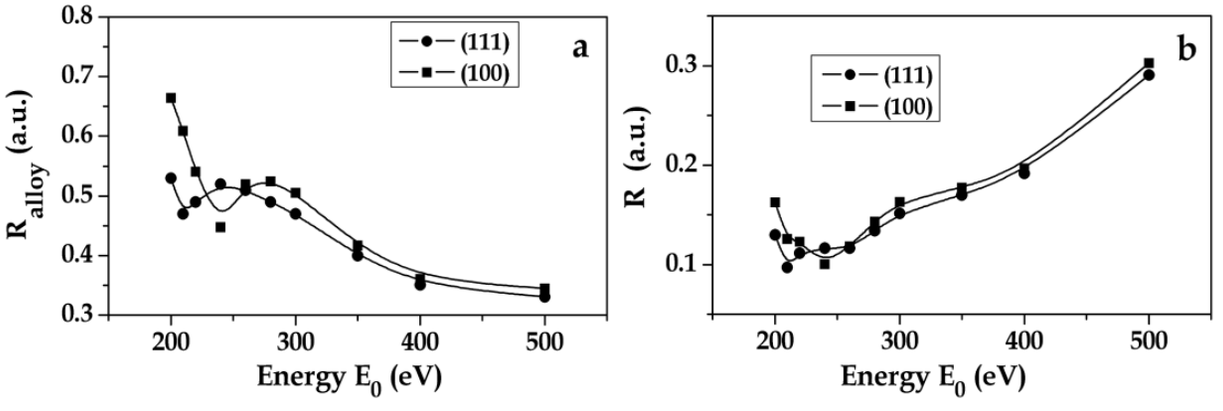

Figure 4. The ratio of ionization peaks of Co to Pt as a function of the primary electron energy for (111) and (100) faces of $Pt_{80}Co_{20}$ alloy at room temperature: (a) – before and (b) – after normalization on the standards

Based on experimental data $R(E_0)$, we calculated the layer-by-layer Pt concentration profiles for (100) and (111) faces of alloy $Pt_{80}Co_{20}$ by means of the condition–gradients projection method, the conjugate gradients projection method, the method of conjugate gradient projected on the Π^+–space with total level of experimental errors less than 3%. On Figure 5 the averaged Pt concentration are shows to all three methods by histograms.

It can be seen that the upper layer contains only platinum atoms for both faces and practically does not contain cobalt atoms. Moreover, there are strong orientation effects that affect on length of the platinum concentration oscillations for the (100) and (111) faces. The deeper oscillation is observed for a more "loose" (100) face, which affects the depth composition up to eight atomic layers. Whereas for the close-packed (111) face these changes are damped on the fifth level. The presented results are in good agreement with experimental data of concentration profiles which were obtained by means of LEED and LEIS [13,14].

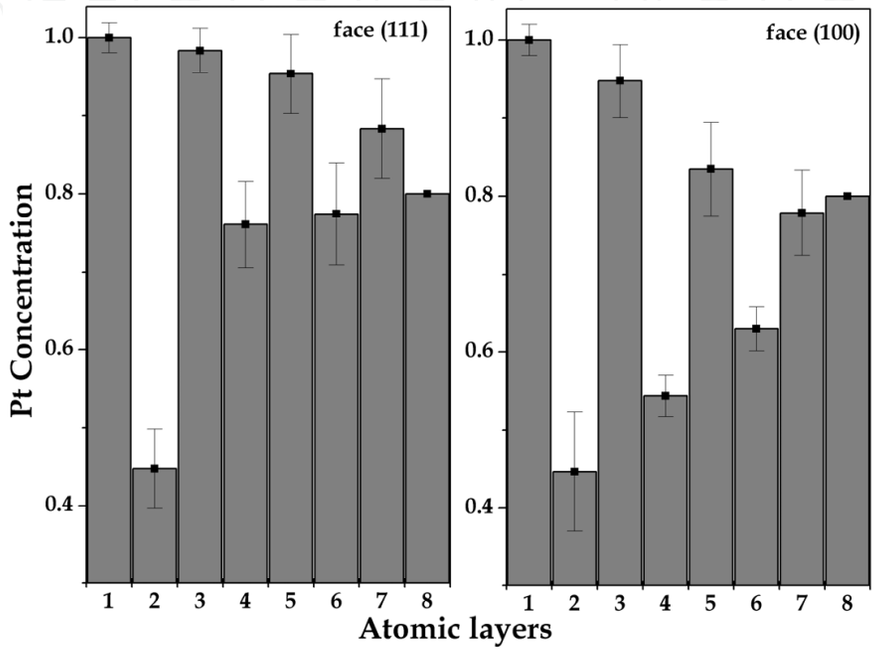

Figure 5. Layer-by-layer Pt concentration profiles reconstructed from the ionization spectra for (111) and (100) faces of $Pt_{80}Co_{20}$ alloy at room temperature

Non-destructive method of layer-by-layer analysis by IS can be effective at study of temperature concentration profiles. Authors [8] investigated influence of heating on concentration profile of $Pt_{80}Co_{20}$(111) (see Figure 6). Heating the sample to 613 K leads to a depletion of Pt atoms in the 2nd layer ($C_{Pt}^{(2)}$ = 24%) and to an insignificant enrichment of Co atoms in layers 3-6 in comparison with the profile at room temperature. Increasing the temperature further to 673 K is accompanied by a negligible segregation of Co from the second layer ($C_{Pt}^{(2)}$ =31%) to the first ($C_{Pt}^{(1)}$ = 97%), while deeper layers remain practically unchanged. At 823K, a sandwich-like structure of the type Pt/Co/Pt was found in the first three atomic layers. As is obvious from Figure 6, heating the sample causes a smoothing of the oscillations in deeper layers towards the bulk concentration of the alloy. However, the first layer still consists of pure Pt up to 873 K. Further increasing the temperature gradually results in completely smoothed oscillations.

Consequently, the sample was slowly cooled during 10 hours from 1123 K to room temperature. As a result of this procedure, a chemically ordered alloy surface of the $L1_2$ type was obtained. LEED shows super-structural reflections in a diffraction pattern at E_0 = 112 eV. The result of the layer-by-layer reconstruction for the ordered state shows that the 1st

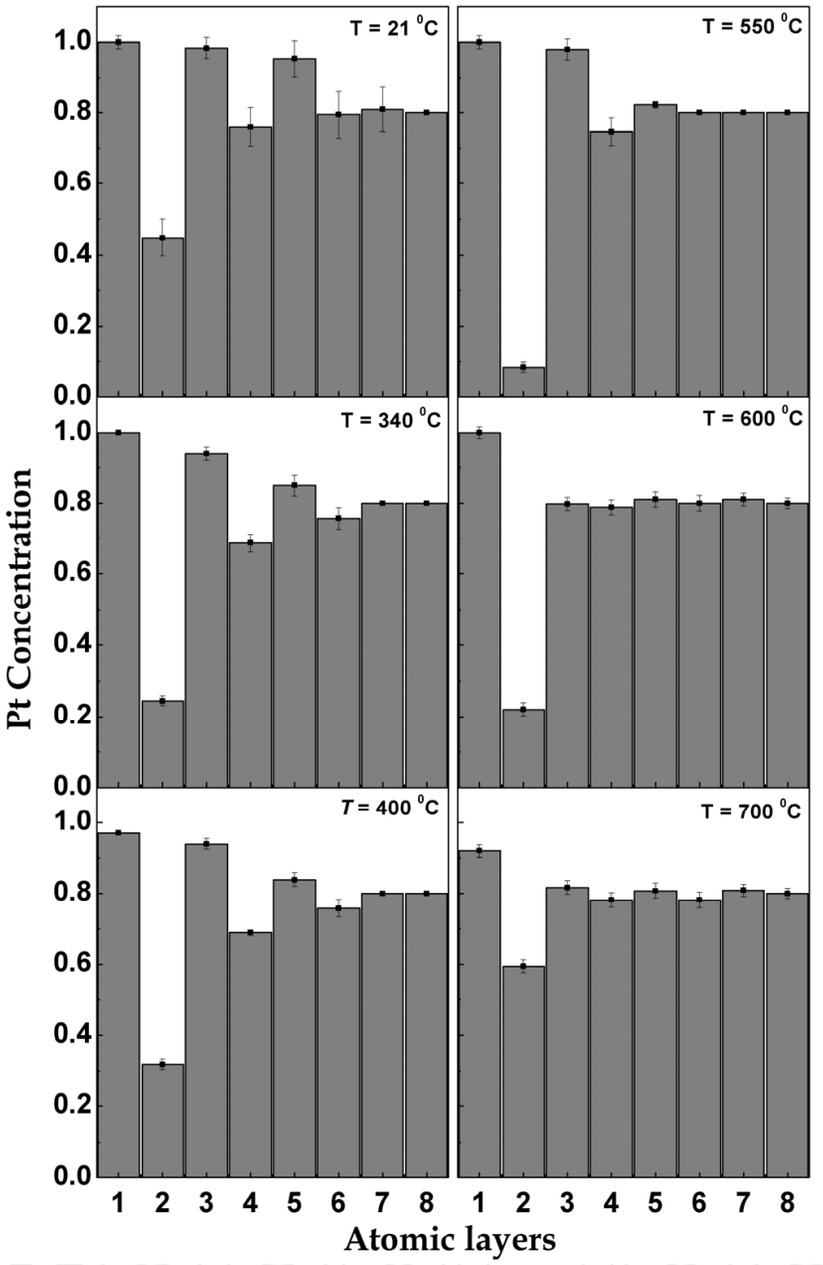

Figure 6. Layer-by-layer Pt concentration profiles reconstructed from the ionization spectra for the $Pt_{80}Co_{20}(111)$ alloy at the different heating

atomic layer consists of pure platinum, and that the other atomic layers have concentrations near the bulk value of the alloy. Probing the surface with primary electrons of 58 eV (corresponding to a probing depth of two atomic monolayers [9]), a p(2x2) structure was found. The appearance of these additional super-structural reflections in a diffraction pattern can be caused by two possible phenomena: chemical ordering at the surface of the alloy and/or a reconstruction of the surface [14].

In work [15] Electron Energy Loss Spectroscopy has been employed for investigation of the effect of 600 eV Ar^+-ion irradiation in the dose range $7{\cdot}10^{16}$–$4{\cdot}10^{17}$ ions/cm^2 on the atomic structure and surface composition of $Pt_{80}Co_{20}(111)$ alloy. Using the ionization energy loss

spectra, a layer-by-layer concentration profile of the alloy components was reconstructed for different doses of ion irradiation of the surface. The Ar^+-ion bombardment of the alloy was found to result in the preferential sputtering of Co and in the enrichment of the near-surface region by Pt atoms with formation of an altered layer, which is characterized by a non-monotonic concentration profile dependent on the irradiation dose. The results obtained are discussed in the framework of the models of preferential sputtering and radiation-induced segregation.

Application of IS for the investigation of composition changes on the depth is not limited to the study by single crystal alloys. In references [8,16] IS was used to study the surface segregation in the ternary Co–Cr–Mo system. Since it was polycrystalline alloy, there can't be applied layer-by layer analysis with profile reconstruction. Nevertheless, the integral distribution of elements on the probing depth can be investigated by means of IS.

According to reference [16] the concentration of the Co–Cr–Mo alloy components on E_0 can be calculated by following expression

$$C_i = \frac{I_i(E_0) / I_i^{st}(E_0)}{\sum_{i=\mathrm{Co,Cr,Mo}} I_i(E_0) / I_i^{st}(E_0)}, \tag{12}$$

where i = Co, Cr and Mo metals, $I_i(E_0)$ and $I_i^{st}(E_0)$ are intensity lines of the ionization losses of the alloy components and standards, respectively. For the thermodynamic equilibrium state the ionization spectra of the alloy components at different temperatures were measured. The condition of the thermodynamical steady–state of the alloy depended on the prolonged heating of the sample at every preset temperature for 15 hours. Figure 7 shows the concentration dependences $C_{Co,Cr,Mo}$ on E_0 for the polycrystalline alloy at a different heating temperatures.

At first, we estimated the thickness of the probing layers for Co-Cr-Mo alloy at change of E_0 from 200 eV to 800 eV. For estimation of the probing depth we used experimental data for the inelastic mean free path (IMFP) λ which are collected in reviews [9] for pure Co, Cr, Mo metals. After, these data was approximated by following equation

$$\lambda = kE_0^{\,n}, \tag{13}$$

where k, n are fitting parameters. As result k = 0.36 and n = 0.5 and variation $\lambda(E_0)$ is from 5Å to 10Å.

For the non–annealed Co–Cr–Mo alloy the Mo atoms showed preferred segregation in the outermost layers at a room temperature. Gradual increase of the probing depth by changing the primary electron energy E_0 to 600 eV shows that the Mo concentration in the near-surface region decreases and the Cr concentration greatly increases, while the Co concentration does not exceed 5–7 at.%. However, at the energy E_0 = 200 eV it was detected that $C_{Co} \approx 42$ at%, $C_{Cr} \approx 20$ at% and $C_{Mo} \approx 38$ at% were present in the near-surface layers.

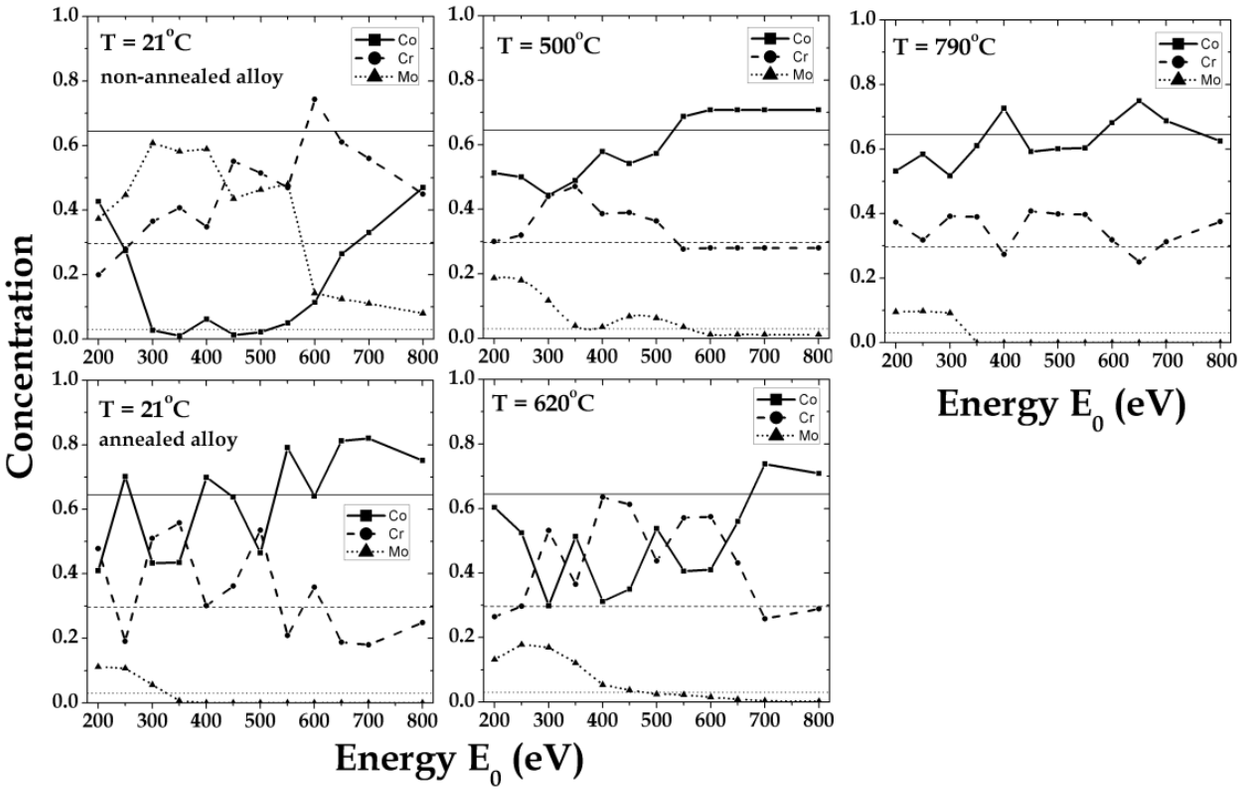

Figure 7. Concentration profiles of Co, Cr, Mo for the Co-Cr-Mo alloy at the different heating by means IS. Horizontal lines are bulk concentration for Co, Cr and Mo, respectively.

On the other hand, for an increase of probing depth at $E_0 > 250$ eV , the concentration of Co atoms sharply decreases to 1–6 at% in the below-surface region at $E_0 = 250 – 550$ eV. With the increase of primary electron energy $E_0 > 600$ eV the Co concentration rises but that of Cr and Mo atoms falls. Only an approximate tendency $C_{Co,Cr,Mo}$ towards the bulk concentration of the alloy is observed at $E_0 = 800$ eV. Heating of the alloy to temperature T = 500ºC essentially induced a change of the surface concentration in the Co–Cr–Mo alloy as compared to the surface concentration for the non–annealed state. Thus, the near surface layers contain $C_{Co} \approx$ 51 at%, $C_{Cr} \approx 30$ at% and $C_{Mo} \approx 19$ at% at the energy $E_0 = 200$ eV. With an increase of the probing depth the Mo concentration is lowered and the concentration of Co atoms is increased. Whereas in the interval of the energies $E_0 = 250 – 400$ eV the sharp growth of Cr concentration is observed and at $E_0 > 550$ eV the alloy composition is close to the bulk value. Further heating of alloy to T = 620ºC promotes an increase in concentration of Co atoms in the near surface region of Co–Cr–Mo alloy (at the $E_0 = 200$ eV). At the primary electron energy $E_0 = 250 – 650$ eV in the deeper layers growth in Cr concentration is detected as compared to the Cr bulk value and only at energy $E_0 > 700$ eV the composition of the alloy comes towards that of the bulk. Further increase of the alloy heating temperature to T = 790ºC is accompanied by smoothing of the alloy composition to the bulk. Nevertheless, an insignificant Mo segregation was still detected in the outermost layers of the alloy.

After prolonged annealing at T = 790ºC the ternary Co–Cr–Mo alloy was slowly cooled to room temperature over 12 hours. The concentration profile for the annealed alloy is shown

on Figure 7. Also for the annealed state the preferred segregation of the Mo and Cr atoms is observed. At the energy E_0 = 200 eV the outermost layers contain $C_{Co} \approx 40$ at%, $C_{Cr} \approx 50$ at% and $C_{Mo} \approx 10$ at%. At increasing primary electron energy E_0 the Mo concentration sharply diminishes and at $E_0 > 400$ eV Mo atoms are not detected anymore, though insignificant oscillations of the composition for the Cr and Co atoms are found near to the bulk concentration at varying E_0. We suggest that the thermodynamic steady–state of the alloy corresponds to that of the annealed alloy at room temperature, but not for the non–annealed alloy.

2.2. Kinetics of surface segregation by IS

IS can be effective at investigation of kinetic processes in the thin layers of a solid. In work [17] for studying kinetics of surface segregation of the $Pt_{80}Co_{20}(111)$ alloy, the temperature interval T = 613 - 973K (T = 340 - 700 °C) is chosen at which the bulk alloy is in the ordered state. A special device allowed heating the sample to predetermined temperature, keeping it constant and changing with an accuracy ±2°C. Platinum - Pt alloy and 1%Rh thermo-couple was welded to the investigated sample for control temperature. Spectra of ionization losses were measured at every chosen temperature with a fixed time interval for platinum ($\Delta E^{Pt}_{O_{2,3}} = 54eV$) and cobalt ($\Delta E^{Co}_{M_{2,3}} = 62eV$). Primary electron beam with energy E_0 = 250 eV was taken for surface probing which by converting into monatomic layers corresponds to the 3rd monatomic layer over the depth [8]. Figure 8 shows the kinetics of segregation for Pt and Co atoms in the near-surface region at different temperatures of $Pt_{80}Co_{20}(111)$ alloy.

Note, that diffusion processes (internal diffusion) for single crystal alloys course mainly according to the vacancy mechanism [1]. Under heating up to 613K the kinetics of segregation atom $C_\beta(t)$ has a classical dependence which may be provisionally divided into two regions: I is the region of fast diffusion when strong segregation of Co atoms is observed; II is the saturation region when the steady-state equilibrium of segregating atoms is set in the near surface alloy region. The character of kinetic curve $C_\beta(t)$ dependence changes substantially at higher temperatures. Thus, when heating is up to 673K the fast diffusion region I has more gentle appearance and region II acquires two characteristic sites: IIa is the region of changing the direction of Pt and Co atoms segregation (temporary S-shaped fold), smoothly transient into IIb, which is region of steady-state equilibrium of segregating elements. We consider that such S-shaped fold is associated with eventual formation of the ordered phase in the near surface region. One of the reasons for nucleation of the composition close to the ordering is a decrease of interatomic interaction constants and as the consequence, an increase of the amplitude of thermal atomic oscillations. We suppose that, most probably, an ordered phase is formed between the 3-5th atomic layers. Since at probing of the alloy surface by electrons with the energy E_0 = 200 eV (1-2nd monolayer [8]), the integral concentration of Pt and Co atoms was C_{Pt} = 0.9 at.% and C_{Co}= 0.1 at.% within the whole time and temperature interval. This confirms the preferred segregation of Pt atoms in topmost layers. The further increase temperature for $Pt_{80}Co_{20}(111)$ alloy will lead to growth of the vacancies number due to

thermal oscillation expansion of atoms and hence it will accelerate diffusion processes. Heating of alloy up to 823K, especially at 873K, leads to increase Co atoms enrichment in the near-surface alloy region as compared to other heating temperatures, and to decrease time which needed for the possible alloy ordering (IIa region). At heating of sample higher ordering temperature the rapid segregation of Co atoms was observed in region I which soon will be replaced by the segregation of atoms Pt (region II) and tend to bulk concentration. Such character of temporal diffusion of cobalt and subsequent segregation of platinum we suppose with redistribution of atoms in the near surface region of alloy.

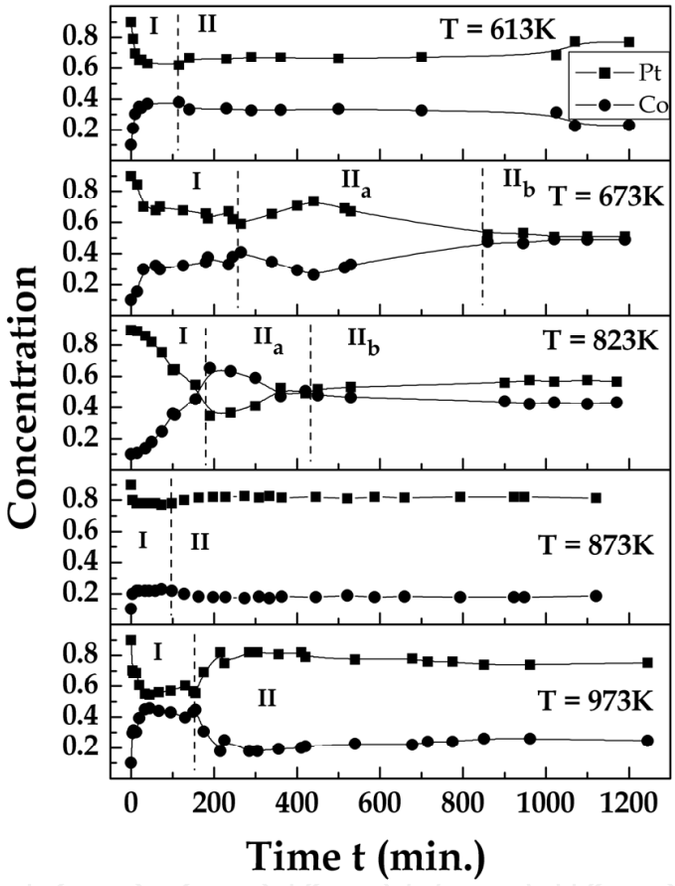

Figure 8. Kinetics of surface segregation in the near surface region for $Pt_{80}Co_{20}$(111) alloy at different heating

At studying kinetics of segregation of the binary alloys in the work [18] was established that the concentration C_x^t of segregating atoms to the surface from the bulk for the time t out of the depth x may be given by the following ratio:

$$C_x^t = C_\infty - C_\infty\left(1-\frac{1}{\alpha}\right)\exp\left(\frac{x}{\alpha d}+\frac{Dt}{\alpha^2 d^2}\right)erfc\left[\frac{x}{\sqrt{4Dt}}+\left(\frac{Dt}{\alpha^2 d^2}\right)^{1/2}\right], \quad (14)$$

where C_∞ is the bulk concentration of diffusing atoms; D is the diffusion coefficient; d is the thickness of the surface layer; α is the degree of surface enrichment defined as

$$C_s^t = \alpha C_0^t, \tag{15}$$

where C_s^t is the concentration of segregating atoms in the surface region; C_0^t is the atom concentration at the depth d at the initial time. By comparing formula (14) and (15) provided that α >>1, we get

$$C_x^t = \alpha C_\infty \left[1 - \exp\left(\frac{Dt}{\alpha^2 d^2} \right) erfc\left(\frac{Dt}{\alpha^2 d^2} \right)^{1/2} \right]. \tag{16}$$

Data approximation of the kinetics of segregation atoms cobalt by Eq. (16) allowed to determine the mean coefficient values of cobalt diffusion at different temperatures, the order of which corresponds to diffusion bulk values. According to these results, the temperature dependence of Co diffusion coefficient in $Pt_{80}Co_{20}$(111) alloy was plotted (Figure 9), by which pre-exponential factor D_0= 5.1 m^2 s^{-1} and energy activation E = (327±22) kJ/mol were determined. The value of energy activation is close to sublimation heat of pure cobalt E = 309.73 kJ/mol.

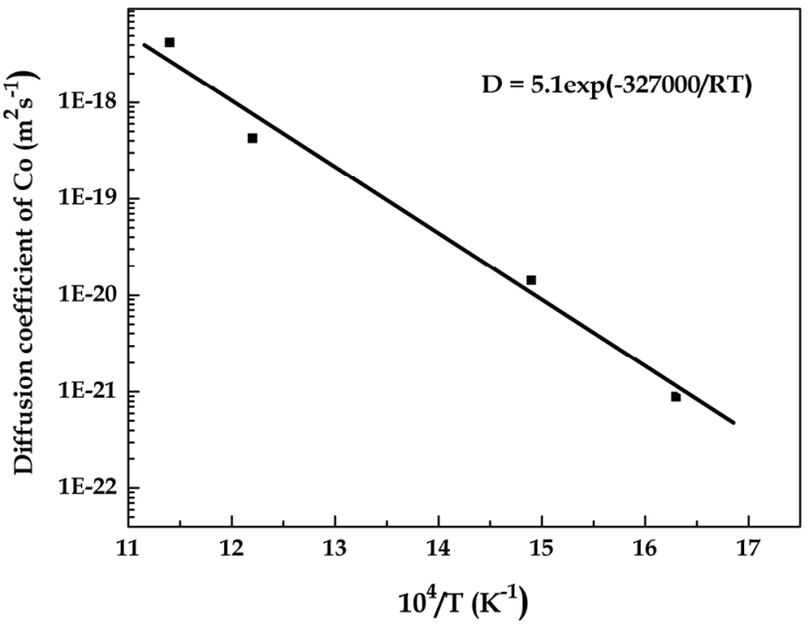

Figure 9. Diffusion coefficient of Co atoms in $Pt_{80}Co_{20}$(111) alloy surface

2.3. Plasmon excitation

Plasmon excitations are potential data carriers about composition and chemical state of elements on the surface and bulk of solid and in the adsorbed layers.

2.3.1. Plasmon energy

A longitudinal plasma wave along the crystal produces long–range Coulomb forces between positive and negative charges and excites collective oscillations. These are called plasmons

in the case of a free–electron gas model. The plasmon energy is obtained from the Fourier modes of the electron density $\rho(r) = \sum_k \rho_k e^{-ik\cdot r}$ and the ϱ_k are amplitudes of harmonic density fluctuations obeying [3]:

$$\ddot{\rho}_k + \omega_p \rho_k = 0 \tag{17}$$

in which ω_p is the Langmuir frequency. Then plasmon energy can be determined by the following expression:

$$E_b = \hbar\omega_b = \hbar\sqrt{\frac{e^2 N}{m\varepsilon_0}}, \tag{18}$$

where $\hbar$ is Plank's constant; ω_b is the cycle frequency of the bulk plasmon; e and m are the electronic charge and mass, respectively; n is the number of valence electrons per unit volume and ε_0 is the permittivity of the free space. The surface plasmon energy E_s is related to bulk plasmon energy by the following equation [19]:

$$E_s = E_b / \sqrt{1+\varepsilon_s}, \tag{19}$$

where ε_s is the dielectric constant. In the framework of the model under consideration, $\varepsilon_s = 1$, i.e. $E_s = E_b / \sqrt{2}$.

In references [5, 20-24] the surface and bulk plasmon excitations were investigated for the $Pt_{80}Co_{20}$(111) and $Cu_{75}Pd_{25}$(100) single crystal alloys, ternary Co–Cr–Mo alloy and amorphous and crystalline $Fe_{73.6}Cu_1Nb_{2.4}Si_{15.8}B_{7.2}$ (FINEMET) alloy surface and their alloy components in range primary electron energy E_0 from 150 eV to 800 eV. It was found that the experimental values of plasma oscillation energy for all pure elements differ from the theoretical calculations but the data obtained in the given works are in good agreement with the results obtained by other authors.

Actually, the difference between experimental data and the free–electron gas model has been observed repeatedly for a lot of chemical elements. This may be a result of: (i) incomplete participation of valence electrons in the collective excitations; (ii) the involvement of filled d-band states and the appearance of inter– or intra-band transitions in characteristic spectra for the transition metals; (iii) cleanness and roughness of the surface region of specimens [3].

For example, on Figure 10 the bulk plasmon energies are shown for the range of primary electron beam energy 150 – 650 eV for pure Fe, Si, B, Nb, Cu and $Fe_{73.6}Cu_1Nb_{2.4}Si_{15.8}B_{7.2}$ alloy. It is known that, for silicon, the surface and bulk plasmon energy are 12 eV and 17 eV, respectively [4]. In our experimental data the plasmon energies are ~ 9 eV and ~15 eV. Most probably the shift of plasmon energies toward lower energy is related to the surface effects when comparing with other work because the probing depth is not deep and varied from 5.4 Å – 5 Å for silicon in the chosen range of E_0. Appearance of silicon oxides on the surface there can be eliminated since forming of oxides would lead to considerable increase in

plasmon energy. For preparation of an atomically clean surface the amorphised silicon surface was first bombarded by argon ions and, subsequently, the sample was annealed at a high temperature. Consequently, both amorphous and crystalline phases can exist in the surface layers of Si. Also we cannot eliminate the fact that residual defects and implanted ions of argon may exist in the near-surface region, which is caused by ion irradiation. In the case of silicon we suggest that the total contribution of the above-mentioned surface effects will influence the shift of energy of plasma excitations to a lower energy. The experiments showed that, for the pure Fe, Si, B, Nb and Cu, the plasmon energy relation E_b/E_s exceeds the theoretical values and is equal to 1.79, 1.67, 2.13, 1.78 and 1.27, respectively. This discrepancy between theory and experiment has been observed repeatedly for many metals [3]. It should be noted that the theory supposes a perfectly flat surface in the vacuum–solid region and does not take into consideration the real physical–chemical state of the metallic surfaces.

According to reference [24] the experimental number of the valence electrons per unit volume n_{alloy} for the amorphous $Fe_{73.6}Cu_1Nb_{2.4}Si_{15.8}B_{7.2}$ alloy on E_0 can be calculated by the following expression

$$n_{\text{alloy}}(E_0) = \sum_{\text{j}} N_{\text{j}}\, n_{\text{j}}(E_0)\,, \tag{20}$$

where j = Fe, Si, B, Nb and Cu metals; N_j is number of the j–atoms per unit bulk (in our approach for the amorphous state, it is a bulk atomic concentration of the alloy components); $n_{\text{j}}(E_0)$ is the experimental number of the valence electrons per unit volume of the pure j–elements at fixed energy E_0. Substituting Eq.(20) into Eq.(18) and using experimental data we calculated the surface and bulk plasmon energy depending on primary electron energy E_0. The results of the calculations for the bulk plasmon energy of FINEMET are shown in Figure 10.

The obtained results are in good agreement with experimental data. For the surface plasmon the design function $E_s(E_0)$ is localized between values for the amorphous and crystalline alloy whereas for $E_b(E_0)$ there is a different situation. At low average primary electron energy $E_0 < 200$ eV the calculated function $E_b(E_0)$ is absolutely identical to energies of the bulk plasmon for the amorphous alloy and at energy $E_0 > 250$ eV the function $E_b(E_0)$ is close to the experimental data E_b for the crystalline state of the alloy. It was observed that, for the crystalline alloy, the energy of plasmon excitations is localized at lower loss energies as compared to those for the amorphous state.

It is known that the electronic state densities in the surface layers can be induced by such an effect as surface segregation. These phenomena are typical for major complex alloys when the composition in the near surface region differs from the bulk composition and it is caused by minimization of the free surface energy of the alloy [1]. Therefore the crystalline and phase structure and altered surface layers will also influence the dispersion of the surface and bulk plasmons when changing the primary E_0 or probing depth on amorphous or crystalline states of the alloy.

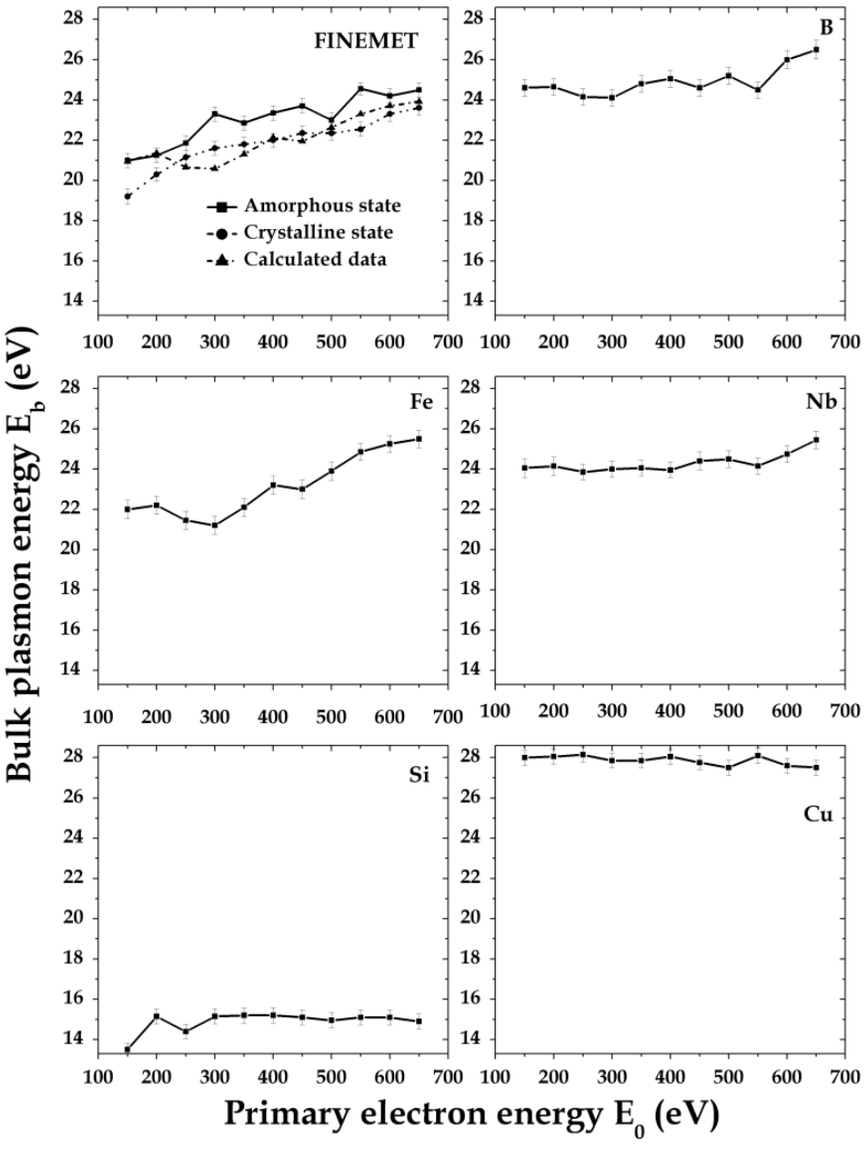

Figure 10. Dependence of the bulk plasmon energy E_b on the primary electron energy E_0 for the $Fe_{73.6}Cu_1Nb_{2.4}Si_{15.8}B_{7.2}$ alloy ribbons surface and pure alloy components

Similarly situation was observed at study plasmon energies for the disordered and ordered states of $Pt_{80}Co_{20}(111)$ alloy where are E_s = 10.57 eV, E_b = 22.17 eV and E_s = 15.8eV, E_b = 25.31 eV, respectively [21,22]. The plasma oscillations for the disordered state are localized at lower loss energies than it was established for ordered state. For the ordered alloy the bulk plasmon energy is 2–3eV more than that of the disordered alloy, whereas the difference for the surface plasmon energy is 4–7 eV in the whole range E_0. Probably it is related to changes of the DOS of valence electrons at the ordering alloy and surface segregation in the atomic layers.

Surface and bulk plasmon energy is sensitive not only to surface segregation, phase state etc but to heating too. EELS has been employed for investigation of the surface and bulk plasmon excitations versus heating in the Co–Cr–Mo alloy surface for the primary electron beam energies E_0 ranging from 150 to 800 eV (see Figure 11) [23].

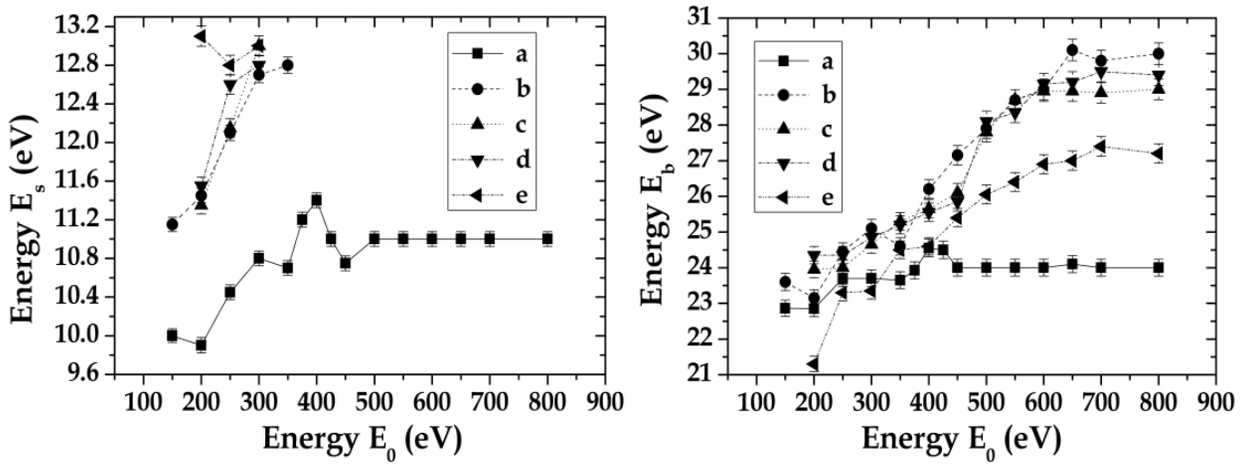

Figure 11. Dependence of surface and bulk plasmons energy from the primary electron energy E_0 for the Co-Cr-Mo alloy at different heating: (a) non-annealed state at T = 21 °C, (b) annealed state at T = 21 °C, (c) T = 500 °C, (d) T = 620 °C, (e) T = 790 °C.

As shown on Figure 11 for the annealed alloy the energies of surface plasmon E_s and bulk plasmon E_b are localized at greater energies than for the non–annealed alloy. In the range of the primary electron energy E_0 = 150 – 800 eV for the surface plasmon E_s this difference is 1 – 2 eV. For the (non–)annealed alloy at room temperature the surface plasmon energy E_s have a linearly growth with a increase of the probing depth of alloy. Significant changes of bulk plasmon energy was observed for the annealed alloy in the range of the primary electron energy E_0 = 150 – 800 eV. For the non–annealed alloy in this energy range of E_0 the bulk plasmon is varied in small region of energy E_b = 22.8–24.5 eV, whereas it strongly changes for E_b = 23.1–30.1 eV in case of annealed alloy. For the (non–)annealed alloy the plasmon energies E_b are close in the energy range E_0 = 150 – 200 eV. With an increase of primary electron energy E_0 for the annealed alloy the bulk plasmon energy linearly increases and remains unchanging at E_0 > 650 eV.

At heating the surface plasmon energy E_s is shifted with an increase of the energy, and than more temperature of sample the more shift of energy E_s. However, the energy shift of surface plasmon, which is induced by heating there strongly differs against to annealed and non–annealed states of alloy. In all region of heating of the ternary Co–Cr–Mo alloy the energy of bulk oscillation E_b increases linearly with an increase of the primary electron energy E_0. With respect to dependence E_b from E_0 for the annealed state the alloy heating to temperatures 500ºC and 620ºC it is accompanied by growth of plasma energy E_b in the range of the energy E_0 = 150 – 350 eV (the near surface region) and decrease this value at the E_0 > 400 eV. Further heating of alloy to T = 790ºC promotes to an insignificant shift of long wavelength plasmon oscillations E_b to sideways decrease of their energy in all region of E_0 as compared to other temperatures of Co–Cr–Mo alloy. Thus, for example, at the temperatures 500ºC and 620ºC the difference of bulk plasmon energy from 0.1 eV to 1.2 eV modulo with respect to annealed alloy, whereas at T = 790ºC it changes from 0 eV to 2.7 eV at corresponding energies E_0. In the range of the primary electron energy E_0 > 650 eV the bulk plasmon energy E_b has a linearly dependence in all temperature regions. We suppose

that this value will correspond to the real bulk plasmon energy crystal at the given temperature of heating.

The authors [25–34] investigated the influence of heating on EEL spectra from the surface of pure elements: C, Al, Ni, Mo, Ta, Pb, Nb, W and Ag. It was observed that owing to heating the surface and bulk plasmon energy suffers shifts in the characteristic spectra. After leaded systematic analysis of this effect by means of Transmission Electron Microscopy with EELS detector, a method of definition of the linear expansion coefficient was proposed using data to thermo–induced shifts of long wavelength plasmons [25–29]. This approach was based on the supposition that at heating of metal in consequence of the expansion/compression of crystal lattice the conductive electron density will lower/raise as a result it must lead to decrease/increase plasmon energy. In this case, number of valence electrons per unit n(T) changes due to the thermal expansion of the crystal, Eq. (18) is rewritten using the linear thermal expansion coefficient α(T) of the crystal as follows:

$$\begin{aligned} E_b(T) &= E_b(T_0)\left\{1-\frac{2}{3}\int_{T_0}^{T}\alpha(T')dT'\right\}, \\ E_b(T_0) &= \hbar\sqrt{\frac{e^2 n(T_0)}{m\varepsilon_0}} \end{aligned} \quad . \tag{21}$$

The obtained results for the thermal expansion coefficient are in a good agreement with tabular data for the clean Al, Ag and Pb. Also angular–resolved high resolution EELS was applied to study the plasmon excitations in the spectra of poly and single crystals as a function of temperature T. For example, in Ref. [33] a particular attention was devoted to silver because of the presence of an extremely sharp surface plasmon as observed for thin films and for all low Miller index surfaces. It was established that energy displacement of surface plasmon depends on temperature because of thermal expansion of the solid. Though Jensen et al. [34] observed with EELS strong temperature effects on the surface plasmon energy on graphite, which have been explained as a consequence of the unusual semimetallic band structure. Therefore this approach does not give us an ambiguous explanation of the reason for the plasmon shift in the ternary Co–Cr–Mo alloy. As noted above, the heating of alloy to T = 620ºC promotes to an increase of the bulk plasmon energy with respect to the annealed alloy and only at T = 790ºC the bulk plasmon suffers shift with a decrease of energy. More over, this approach doesn't take into account changes of the surface plasmon energy and their coupling with bulk plasmon in the near surface region.

It is known that the electrons in metals, which are neutralized by the fixed positive ions tightly sufficiently coupled between themselves and disposed in the lattice site, it is possible to consider as the special type of plasma [3]. From the classical point view the plasma oscillations in metals are oscillations of valence electrons with respect to positive ions which formed the lattice. These oscillations are conditioned owing to long–range Coulomb forces. Therefore, besides of the crystal lattice parameter at heating of ternary Co–Cr–Mo alloy it is necessary to take into account the change of Coulomb interaction force between the plasmons and atomic core that can not be calculated within the framework of the classic

approach. The chemical elements Co and Cr are metals for which either the valence electrons are strongly bond s, d–electrons and the core electrons are weakly bond. Probably that at change of heating of these metals and those alloys the shift of plasmon energy with an increase or decrease of energy also will be determined by the change of Coulomb interaction force between the valence electrons and the core. It can lead to change of free s, d–electron concentration and effective electronic mass m (in Eq.(18)), which do participate in plasma excitations and, as a result, to shift the plasmon loss line relative to initial state of Co–Cr–Mo alloy.

Fact, for the pure chemical elements the surface and bulk plasmon energy can substantially differ from the plasmon energies of their alloys or compounds. In reference [16] was observed that in the near surface region the profile concentration versus temperature is differs to bulk of ternary Co–Cr–Mo alloy. Therefore, it is necessary to expect a displacement of long wavelength plasmon oscillations in the range of the energies E_0 = 150 – 650 eV as a result of segregation of the alloy components. However as far as the changed composition of the near surface region of alloys can strongly influence on plasma excitations at different temperatures at the present time is not clean.

The experimental data obtained in Figure 11 are indicated about the complex nature of the plasmon shifts in the near surface region of ternary Co–Cr–Mo alloy. Although most authors meet an opinion, that the energy plasmon shift mainly can be related to lattice parameter of solids, we suppose that in case of the complicated Co–Cr–Mo system the shift of plasmon energy will be defined by the summary balance of above mentioned possible causes at heating.

2.3.2. Intensity lines of plasmons

The nature of the surface plasmon appearance in the EELS spectra is related to the physical and chemical state of the surface layer nanosize thickness. It is also known that probability of the surface plasmon excitation by primary electrons will be directly related to their probing depth of the solid. Growth of the primary electron energy will lead to the increasing of the bulk plasmon excitation probability and, on the other hand, to the decreasing of the surface plasmon excitation probability and to damping of the surface plasmon intensity line in the EELS spectra. Consequently, for every chemical element and their alloys it is possible to define the range of the primary electron energy, in which the line of the surface plasmon will be detected in the characteristic loss spectra. Based on this concept, in references [20, 21] it was proposed to determine of the ratio R_s (in a.u.) of IL surface and bulk plasmons from the energy E_0 by the following equation:

$$R_{s,b}(E_0) = \frac{I_{pl}^{s,b}(E_0)}{I_{pl}^{s}(E_0) + I_{pl}^{b}(E_0)}, \tag{22}$$

where $I_{pl}^{s,b}$ is IL of the surface and bulk plasmons from primary electron energy E_0.

In works [20 - 24] the changes of IL for surface and bulk plasmon were studied for the $Pt_{80}Co_{20}(111)$ and $Cu_{75}Pd_{25}(100)$ single crystal alloys, ternary Co–Cr–Mo alloy and amorphous and crystalline $Fe_{73.6}Cu_1Nb_{2.4}Si_{15.8}B_{7.2}$ (FINEMET) alloy surface and their alloy components in range primary electron energy E_0 from 150 eV to 800 eV. There was found that damping of the function $R_s(E_0)$ is different for all specimen and different value of the primary electron energy E_0 for which the intensity line of the surface and bulk plasmons are equal. In case of pure elements the damping of function $R_s(E_0)$ is related to a decrease in probability of their excitation dependant on respective probing depth of the near surface layer and contrariwise this increases the probability excitation of the bulk plasmon and with altered near surface layers. In case of alloy, there was advanced a assumption that decay of intensity line of surface plasmon relative to bulk plasmon can be associated with changing of surface composition on the depth for the alloys and it confirms an assumption as to possibility of establishing the range of primary electron energy E_0, at which the electron beam will probe only the near surface region for the different materials.

Good correlation between the damping of surface plasmon $R_s(E_0)$ and concentration profile was established for the $Cu_{75}Pd_{25}(100)$ alloy surface at room temperature [20] and for the $Pt_{80}Co_{20}(111)$ alloy surface and Co–Cr–Mo alloy at a different heating [8, 23].

The results of measurement for $Pt_{80}Co_{20}(111)$ alloy are shown on Figure 12 at different heating. For the disordered alloy the damping of surface plasmon R_s have a more prolonged dependence compared to the ordered alloy at room temperature. If we will estimate a probing depth at primary electron energies E_0 = 550 eV and E_0 = 350 eV when surface plasmon does not appear ($R_s \approx 0$) in the EELS spectra, then we founds approximately 6-7th and 2-3rd atomic layers (bulk concentration) for the disordered and ordered states of $Pt_{80}Co_{20}(111)$ alloy, respectively (see Figure 6).

As in case of thermo–induced shift of plasmon excitations the changes in IL of surface plasmon relative to bulk plasmon were observed. Heating of alloy induces decreasing intensity line of surface plasmon and then higher temperature that more damping of surface plasmon R_s at variation of the primary electron energy E_0. In case of the $Pt_{80}Co_{20}(111)$ alloy surface with increasing of heating the damping of oscillating concentration depth profile is decreases [8]. More over, there is observes correlation between damping of surface plasmon R_s relative to bulk plasmon and damping of oscillating concentration depth profile at every given temperature.

The results of measurement for the Co-Cr-Mo alloy are shown on Figure 13 at different heating. For the non–annealed alloy the damping of surface plasmon R_s has a prolonged dependence and only at $E_0 > 800$ eV the surface plasmon peak disappears in EELS spectra. For the annealed state of alloy with an increase of the energy E_0 the dependence R_s decays quickly compared to the non–annealed alloy and at energy $E_0 > 350 - 400$ eV the surface plasmon does not appears in EELS spectra. As in case of shifts of the surface and bulk plasmon energy at heating of alloy the essential changes on intensity lines of surface plasmon relative to bulk plasmon were observed.

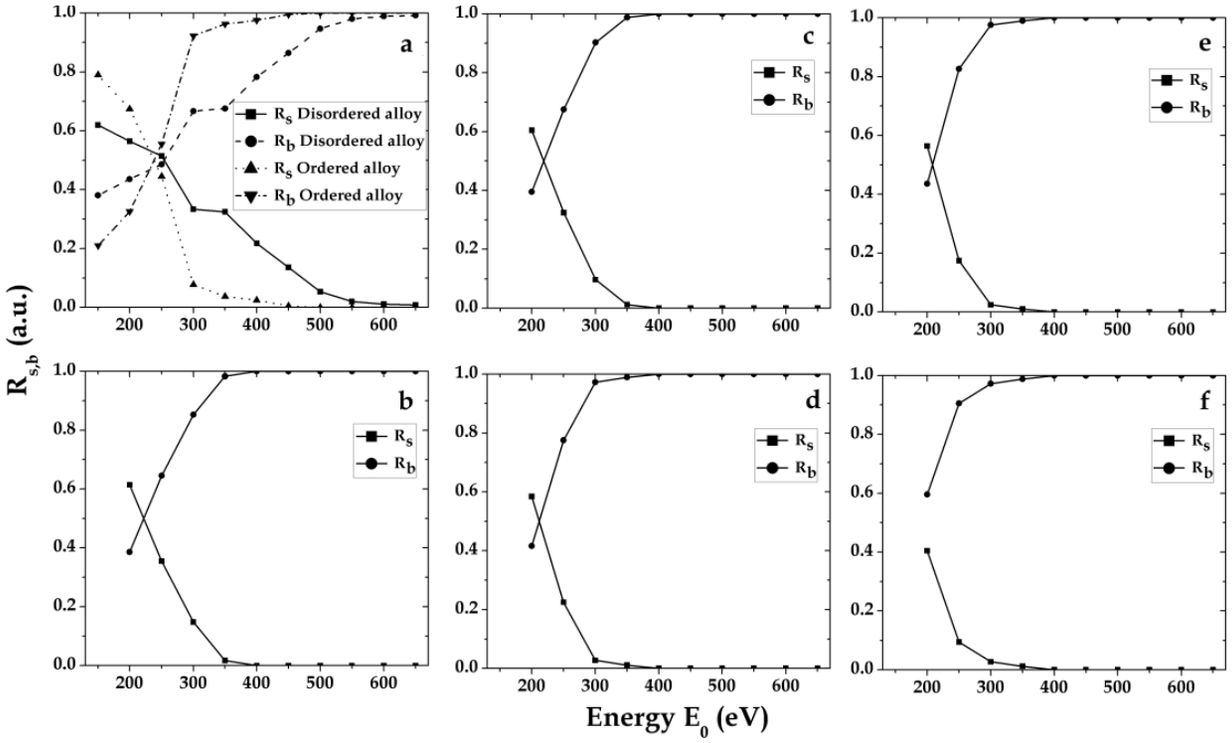

Figure 12. Dependence $R_{s,b}(E_0)$ from the primary electron energy E_0 for the $Pt_{80}Co_{20}(111)$ alloy at different heating: (a) T = 21 °C, (b) T = 340 °C, (c) T = 400 °C, (d) T = 550 °C, (e) T = 600 °C, (f) T = 700 °C

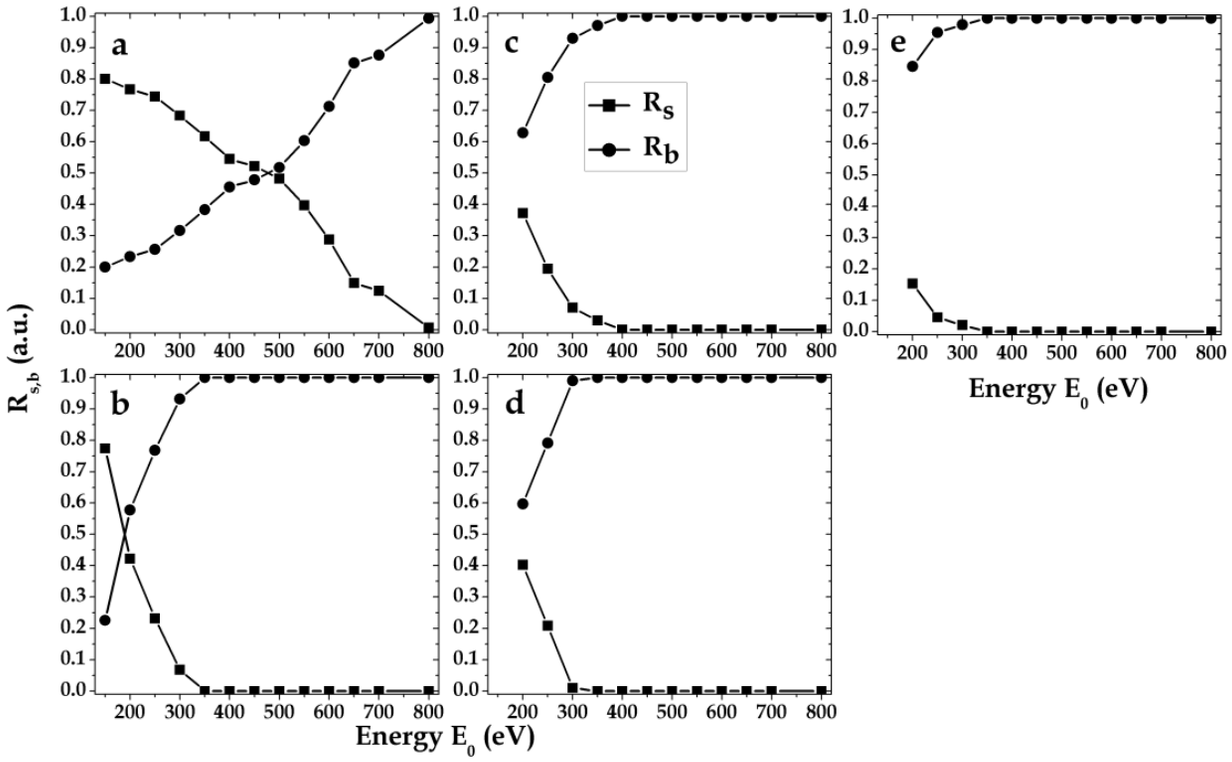

Figure 13. Dependence $R_{s,b}(E_0)$ from the primary electron energy E_0 for the Co-Cr-Mo alloy at different heating: (a) non-annealed state at T = 21 °C, (b) annealed state at T = 21 °C, (c) T = 500 °C, (d) T = 620 °C, (e) T = 790 °C.

Heating of Co-Cr-Mo alloy induces decreasing IL of surface plasmon as well as probability of their appearance in EELS spectra dependence on temperature at variation of the energy E_0. High–temperature heating of Co–Cr–Mo alloy promotes to increase the emission and background of secondary electrons in characteristic spectra, that did not allow us exactly to separate the peaks of plasma oscillations at small primary electron energy E_0 = 150 eV. As shown on Figure 13 for temperatures 500ºC and 620ºC the line of surface plasmon disappearances at E_0 > 350 eV and E_0 > 300 eV, respectively. At heating of alloy to T = 790ºC the surface plasmon is detected only in range of the energy E_0 = 200 – 350 eV, however dependence R_s from E_0 decays quickly compared to other temperatures. Besides increasing the intensity line of plasmons with the increase of heating of Co–Cr–Mo alloy the observed a broadening of bulk plasmon line. The correlation between the damping of function R_s from E_0 and formation of concentration profile in the near surface region of alloy was established for the non–annealed Co–Cr–Mo alloy (see Figure 7). For the annealed alloy the surface plasmon detects in EELS spectra in the range of E_0 = 150 – 350 eV. This range of energy E_0 corresponding to the near surface region where was observed the largest variation of alloy composition relative to bulk concentration. The similar situation occurs at heating to T = 790ºC for which the alloy concentration in the near surface region comes towards to the bulk at energy E_0 > 300 eV. Only the qualitative the correlation between the damping function R_s from E_0 and comes towards to the bulk concentration are observes for the Co–Cr–Mo alloy at the temperatures 500ºC and 620ºC.

3. Conclusion

Low Electron Energy Loss Spectroscopy can be used as effective non-destructive method at investigation of physical-chemical properties materials in the nano-size near surface region.

Ionization energy losses allows to investigation layer-by-layer concentration profile for the singe crystal alloys with monolayer resolution, element distribution on the depth for the polycrystalline alloys and study of kinetics of surface processes at thermo-induced treatment or after ion irradiation of the surface.

Plasmon excitations are very sensitive to structural and chemical state of surface and bulk and it can be used for study of electronic states of free electrons in the near surface region and influence of different kinetic processes on changing of electronic structure of materials.

Analysis of intensity line of surface and bulk plasmons depending on primary electron energy E_0 allows to define a surface-bulk interface when electron beam probes just near surface region with different physical-chemical properties as compared to the bulk material. These results have good correlation with data of surface composition on depth which obtained by IS and AES.

Author details

Vitaliy Tinkov
Department of the Surface Atomic Structure and Dynamic, Institute for Metal Physics of NAS of Ukraine, Ukraine

Acknowledgement

The author would like to acknowledge professor M.A. Vasylyev for his help in discussion this paper.

4. References

[1] Vasiliev, M A. Surface effects of ordering in binary alloys. Journal of Physics D: Applied Physics 1997;30(22) 3037-3070.
[2] O'Connor, D.J., Sexton, B.A. & Smart, R.St.C. Surface Analysis Methods in Materials Science, 2nd edit, Berlin: Springer; 2003.
[3] Raether, H. Excitation of Plasmon and Interband Transitions by Electrons. Springer Tracts Modern Physics 1980;88 1-196.
[4] Lüth, H. Surface and Interfaces of Solids. Springer Series in Surface Science 1993;15 1-356.
[5] Vasylyev, M.A., Tinkov, V.A. & Gurin, P.A.. Electron Energy Loss Spectroscopy study of the near surface region of dental Co–Cr–Mo alloy. Applied Surface Science 2008;254 4671–4680.
[6] Gerlach, R.L., Houston, J.E. & Park, R.L. Ionization spectroscopy of surfaces. Applied Physics Letters 1970;16(4) 147-188.
[7] Gerlach, R.L. Ionization Spectroscopy of Contaminated Metal Surfaces. Journal of Vacuum Science & Technology 1971;8 599-604.
[8] Vasylyev, M.A., Tinkov, V.A., Blaschuk, A.G., Luyten, J. & Creemers, C.. Thermo–stimulated surface segregation in the ordering alloy $Pt_{80}Co_{20}$(111): Experiment and Modeling. Applied Surface Science 2006;253 1081–1089.
[9] Seah, M.P. & Dench, W.A. Quantitative electron spectroscopy of surfaces: A standard data base for electron inelastic mean free paths in solids. Surface and Interface Analysis 1979;1(1) 2-11.
[10] Baschenko, O.A. & Nefedov, V.I. Depth profiling of elements in surface layers of solids based on angular resolved X-ray Photoelectron Spectroscopy. Journal of Electron Spectroscopy and Related Phenomena 1990;53 1 – 18.
[11] Cherkashin, G.Yu. Inverse problem: the concentration depth profile of elements from ARXPS data. Journal of Electron Spectroscopy and Related Phenomena 1995;74 67 – 75.
[12] Vasylyev, M.A., Blaschuk, A.G. & Tinkov, V.A. Reconstruction of concentration profiles in the surface region of $Pt_{80}Co_{20}$ alloy for (100) and (111) faces by means of ionization spectroscopy. Metal Physics and Advanced Technologies 2003;25(12) 1617–1632.
[13] Bardi, U., Atrei, A., Zanazzi, E., Rovida, G. & Ross, P.N. Study of the reconstructed (001) surface of the $Pt_{80}Co_{20}$ alloy. Vacuum 1990;41(1-3).
[14] Gauthier, Y., Baudoing-Savois, R., Bugnard, J.M., Bardi, U. & Atrei, A. Influence of the transition metal and of order on the composition profile of $Pt_{80}M_{20}$(111) (M = Ni, Co, Fe) alloy surfaces: LEED study of $Pt_{80}Co_{20}$(111). Surface Science 1992;276(1-3) 1 – 11.
[15] Vasylyev, M.A., Chenakin, S.P. & Tinkov, V.A. Electron Energy Loss Spectroscopy study of the effect of low–energy Ar^+–ion bombardment on the surface structure and composition of $Pt_{80}Co_{20}$(111) alloy. Vacuum 2005;78 19–26.
[16] Tinkov, V.A., Vasylyev, M.A. & Gurin, A.P. Investigation of the thermo–stimulated surface segregation in the ternary Co–Cr–Mo alloy by means of Ionization Spectroscopy. Vacuum 2009;83 1014–1017.

[17] Vasylyev, M.A., Tinkov, V.A., Sidorenko, S. & Voloshko, S. The temperature dependence of the atoms Co diffusion coefficient in $Pt_{80}Co_{20}$(111) alloy. Defect and Diffusion Forum 2007;265 19–23.
[18] Lea, C. & Seah, M.P. Kinetics of surface segregation. Philosophical Magazine 1977;35(1) 213-228.
[19] Maier, S.A. Plasmonics: Fundamentals and Applications, Springer Science+Business Media LLC; 2007.
[20] Vasylyev, M.A., Tinkov V.A. & Nieuwenhuys, B.E. Electron energy–loss spectroscopy of the metals Pd, Cu and the ordered $Cu_{75}Pd_{25}$(100) alloy. Journal of Electron Spectroscopy and Related Phenomena 2007;159 53–61.
[21] Vasylyev, M.A. & Tinkov, V.A. Low energy electron induced plasmon excitations in the ordering $Pt_{80}Co_{20}$(111) alloy surface. Surface Review and Letters 2008;15(5) 635–640.
[22] Tinkov, V.A. & Vasylyev, M.A. Thermo–induced shift of plasmon energy in electron loss spectra for the ordering $Pt_{80}Co_{20}$(111) alloy surface. Surface Review and Letters 2009;16(2) 249–258.
[23] Tinkov, V.A. & Vasylyev, M.A. Thermo–induced plasmon excitations in the near surface region of ternary Co–Cr–Mo alloy. Vacuum 2011;85(8) 787-791.
[24] Tinkov, V.A., Vasylyev, M.A. & Galstyan, G.G. Low energy electron induced characteristic losses in the $Fe_{73.6}Cu_1Nb_{2.4}Si_{15.8}B_{7.2}$ (FINEMET) alloy surface. Vacuum 2011;85(6) 677-686.
[25] Watanabe, H. Experimental Evidence for the Collective Nature of the Characteristic Energy Loss of Electrons in Solids – Studies on the Dispersion Relation of Plasma Frequency. Journal of the Physical Society of Japan 1956;11(2) 112-119.
[26] Abe, H., Terauchi, M., Kuzuo, R. & Tanaka, M. Temperature Dependence of the Volume-Plasmon Energy in Aluminum. Journal of Electron Microscopy 1992;41(6) 465-468.
[27] Abe, H., Terauchi, M. & Tanaka, M. Temperature Dependence of the Volume-plasmon Energy in Silver. Journal of Electron Microscopy 1995;44(1) 45-48.
[28] Leder, L.B. & Marton, L. Temperature Dependence of the Characteristic Energy Loss of Electrons in Aluminum. Physical Review 1958;122 341–343.
[29] Imbuch, A. & Niedrig, H. Temperature effect on energy loss spectrum of fast electrons in aluminium and lead foils between 3 K and 295 K. Physics Letters A 1970;32(6) 375-376.
[30] Apholte, H.R. & Ulmer, K. Temperaturabhängigkeit der charakterischen energieverluste in niob, molybdän, tantal und wolfram. Physics Letters 1966;22(5) 552-553.
[31] Heimann, B. & Hölzl, J. Variation of Characteristic Energy Losses in the Curie-Temperature Region of Ni (111). Physical Review Letters 1971;26 1573–1575.
[32] Korsukov, V.E. & Lukyanenko, A.S. The surface relaxation of Al as determined by electron energy loss spectroscopy on plasmons. Zeitschrift für Physik B Condensed Matter 1983;53(2) 143-150.
[33] Rocca, M. Low-energy EELS investigation of surface electronic excitations on metals. Surface Science Reports 1995;22(1–2) 1-71.
[34] Jensen, E.T., Palmer, E.E., Allison, W. & Annett, H.F. Temperature-dependent plasmon frequency and linewidth in a semimetal. Physical Review Letters 1991;66 492–495.